# Development of Dual Charging Sources for an Affordable Rechargeable Lantern to Support a Green Environment

## Candidus U. Eya\*, Chikadibia Ugwuijem Daniel and Abonyi Kingsley

Department of Electrical Engineering, University of Nigeria, Nsukka, Enugu, Nigeria
\*Corresponding Author: candidus.eya@unn.edu.ng
(Received 27 March 2025; Revised 22 April 2025; Accepted 2 May 2025; Available online 6 May 2025)

Abstract - This article presents the development of a dual-source charging system for an affordable rechargeable lantern designed to support a green environment. The proposed system integrates waste plastic materials for packaging, used laptop batteries for energy storage, a DC-DC power converter for DC source charging, and an AC-DC power converter for AC source charging. A distinguishing feature of the design is its dual charging capability, which allows the battery to be charged using either an AC or DC source, depending on availabilityunlike conventional systems that typically support only one input type. Although both charging converters are incorporated within the same system, they do not operate simultaneously. Sensors and a control unit detect the available power source and activate the appropriate charging converter. The DC charging path is deactivated when an AC source is detected, and vice versa. When a DC source is available, the system charges the battery using a regulated DC voltage and current via the DC-DC converter. When an AC supply is available, it is rectified and regulated before charging the battery. The proposed system contributes to environmental protection by reducing pollution and mitigating carcinogenic risks, as it repurposes waste plastic bottles in the lantern's packaging, thereby minimizing plastic litter on land and in aquatic environments.

Keywords: Dual-Source Charging, Rechargeable Lantern, Power Converters (AC-DC, DC-DC), Waste Material Utilization, Green Energy Solutions

### I. INTRODUCTION

A rechargeable lantern is a system that converts electrical energy stored in a battery into light energy. The battery may be a lead-acid, nickel-based, lithium-ion, or other battery type. Rechargeable lanterns (RLs) have, for many years, replaced kerosene lanterns [1], gas lamps, and other traditional lighting methods in residential settings. One reason for this widespread adoption is their relatively pollution-free operation. RLs have numerous applications, including night fishing in rural areas, palm wine tapping in south-eastern Nigeria, student exam preparations, kitchen lighting, and more.

#### II. BACKGROUND OF THE STUDY

Various shapes and sizes of rechargeable lanterns are found in many households across Nigeria, both in rural and urban areas, typically utilizing only one charging source-AC power. When there is an AC utility blackout or no AC power supply, these AC-based rechargeable lanterns remain unchanged after discharging. In this study, the proposed system is designed to utilize both AC and DC charging sources to recharge the lantern, though not simultaneously. This approach ensures that the rechargeable lantern remains functional regardless of the available power source. The selection of the charging source is governed by a control mechanism based on the NAND logic principle. When both input sensors (AC and DC) are HIGH, the trigger signal is LOW, and vice versa. If the DC sensor detects a DC input, the DC charging circuit is activated to charge the batteries. Conversely, if the AC sensor detects an AC power supply, the AC input-coupled with rectifiers-is used to charge the batteries.

## III. AIM AND OBJECTIVES OF THE STUDY

The aim of this study is to develop dual-source charging converters for affordable rechargeable lanterns in support of a green environment.

To achieve this aim, the following objectives are pursued:

- a. Utilizing AC and DC sensors to monitor the type of power source supplied to the circuit.
- b. Applying a NAND logic gate, relay, and transistors to activate the appropriate converter for battery charging.
- c. Designing a step-down DC power converter using power diode D1, IGBT power switch Sm, inductor L, and capacitor C to provide regulated DC charging.
- d. Using the input resistance of resistor R and capacitance of capacitor C, connected in parallel, to limit the AC current.
- e. Implementing thyristors and power diodes to construct semi-controlled rectifiers, along with a Zener diode to rectify and regulate the AC voltage, thereby extending battery lifespan when AC supply is detected.

### IV. LITERATURE REVIEW

The electrical power challenges faced by off-grid rural areas persist despite the growth of renewable energy companies, particularly in countries such as Nigeria. Many industry experts advocate for off-grid solar-powered systems as a viable solution. However, as noted by the author in [2], such systems can be prohibitively expensive, with initial costs comparable to, or even exceeding, those of gas-powered electrification. Several researchers have investigated hybrid

renewable energy systems to improve performance stability and reduce costs in grid-connected configurations [3]-[7]. Historically, kerosene and gas lanterns were the primary lighting sources in many communities during the mid-19th century. This changed with the advent of electricity in developed countries in the mid-20th century, which led to various technological advancements. The shift aimed to reduce the prevalence of diseases such as tuberculosis and respiratory illnesses associated with the frequent use of kerosene-powered stoves and lanterns. The transition to electric lighting significantly improved public health and safety by reducing indoor air pollution, enhancing quality of life, and paving the way for further innovations in energy and lighting technologies. Nevertheless, in some parts of Nigeriaand similarly in certain regions of India-kerosene remains a primary lighting source [8]. This reliance highlights the ongoing challenges in accessing reliable electricity and underscores the urgent need for sustainable energy solutions to improve living standards and safety in these regions.

Numerous researchers have published studies on the merits and drawbacks of charging methods and rechargeable lanterns. The authors in [9] focused on estimating and regulating the state of charge (SOC) in batteries within an extended solar system, using a Kalman filter to approximate SOC. The system maintained the SOC within a safe operating range (20%-80%), effectively preventing overcharging and over-discharging. However, it supported only a single charging mode-AC source-and employed expensive packaging materials, which pose a barrier to widespread adoption. This underscores the need for cost-effective alternatives without compromising system performance, as well as exploring multi-source charging options to improve efficiency.

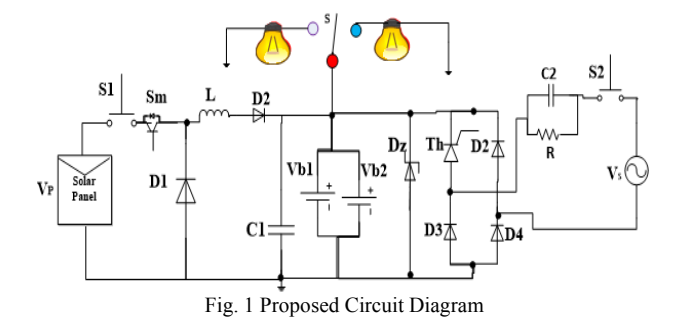
In [10], scholars developed a photovoltaic-powered battery charging system with an inverse current protection mechanism. The design successfully prevented current backflow from the battery to the photovoltaic system. However, it had several limitations, including a humming noise, large physical footprint, and high cost due to the use of a line-frequency transformer. Furthermore, it relied solely on a DC source for charging. To address these limitations, recent research is focusing on transformer less designs that are more compact, quieter, and capable of utilizing both AC and DC charging sources.

According to [11], a system was developed for solar photovoltaic charging of lithium-ion batteries, and its performance efficiencies were evaluated. However, the solar panel directly charged the batteries, a method that poses risks to battery life due to potential overheating and overcharging. Direct charging can significantly shorten battery lifespan, making it essential to implement more controlled and regulated charging techniques. In response to these challenges, this study proposes a low-cost and improved rechargeable lantern designed support to environmental goals. The proposed system is adaptable to both AC and DC power sources, in contrast to conventional

systems that typically include only one built-in charging option. It utilizes waste plastic materials for packaging and repurposed laptop batteries for energy storage. When fully charged, the system can operate continuously for over 16 hours, making it suitable for portable and remote applications. This extended usage time, combined with the sustainable use of waste materials, contributes to reducing landfill waste and promoting environmentally responsible energy practices. The energy conversion process of the proposed system follows this Solar energy (via solar panel) → Electrical energy (through DC-DC buck converter) → Chemical energy (stored in lithium-ion battery)  $\rightarrow$  Light energy (in a bulb). This efficient energy conversion supports diverse applications, including home lighting and outdoor illumination, thereby reducing reliance on conventional energy sources and advancing environmental sustainability.

#### V. METHODOLOGY

A mixed-method approach is employed in this research, combining design, simulation, and experimental methodologies. Fig. 1 illustrates the overall circuit design, which consists of two power sources: a solar panel and an AC power supply. The solar panel section includes a mechanical switch S1, a power diode D1, an inductor L, a unidirectional power diode (also D1), a common filtering capacitor C1, and batteries Vb1 and Vb2. The AC power section comprises the AC source Vs, a mechanical switch S2, current-limiting components (C2 and R), rectifying components (thyristor Th, diodes D2, D3, and D4), and a common Zener diode Dz. The Zener diode maintains voltage regulation across the batteries to prevent overcharging. The proposed system charges the batteries using either the solar panel or the AC supply in a complementary manner. This means that when the solar system is unavailable, the AC power supply can be used to charge the batteries. This dual charging capability ensures that the batteries remain adequately charged at all times. thereby enhancing their lifespan and system reliability. Moreover, the integration of these components enables seamless switching between solar and AC power sources, optimizing energy usage based on availability.



A. Operational Principle of The Proposed System

The proposed system operates in two modes: DC charging operation and AC charging operation. In the DC charging mode, unregulated DC power from the solar supply is

regulated to charge the batteries. In the AC charging mode, AC power is converted to DC power for battery charging.

## B. DC Solar Charging Operation

In the DC charging mode (i.e., when switch S1 is closed), a high, unregulated DC voltage is stepped down to an appropriate level to charge the batteries. The DC charging circuit topology, derived from Fig. 1, is shown in Fig. 2. Fig. 2 illustrates the conversion of solar energy into electrical energy. This electrical energy, in the form of DC power, is periodically converted into chemical energy through the charging process, allowing the batteries to store energy for later use. This efficient energy conversion is essential for optimizing both the performance and lifespan of the batteries within the system.

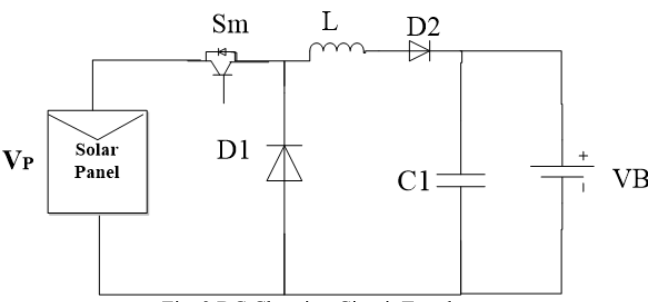
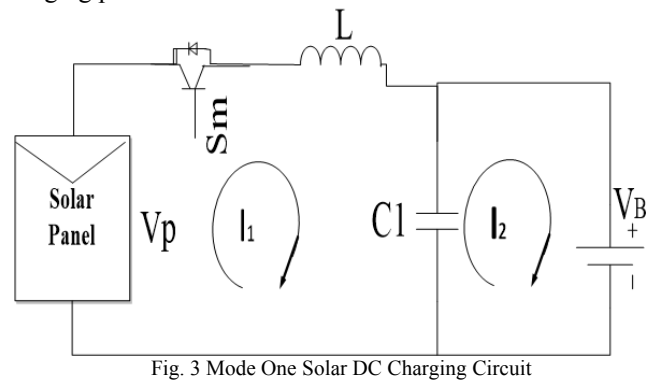


Fig. 2 DC Charging Circuit Topology

The DC charging circuit topology operates in two sub-modes. In the first mode, the temporarily stored magnetic energy in the inductor is discharged to charge the capacitor and supply power to the battery load. In the second mode, magnetic energy is built up in the inductor L, while the electrical energy stored in the capacitor C1 is discharged to the load. The circuit configuration for the first mode is shown in Fig. 3, while the second mode arrangement is presented in Fig. 4. In both configurations, efficient energy transfer is essential for optimizing the performance of the DC charging circuit. By alternating between these two modes, the system maximizes the utilization of stored energy while minimizing losses, thereby enhancing the overall efficiency of the charging process.



During the Mode 1 solar DC charging condition, the power switch is turned ON, while the power diode D1 is reverse-biased. The loop current I1 flows along the following path:

$$Vp \rightarrow Sm \rightarrow L \rightarrow C1 \rightarrow Vp \rightarrow Sm \rightarrow L \rightarrow C1 \rightarrow Vp$$
.

Simultaneously, the current loop in the battery charging path follows:

 $C1 \rightarrow VB \rightarrow C1 \rightarrow VB \rightarrow C1$ . The voltage, current, and impedance relationships for this mode are expressed in Eq. (1).

$$\begin{bmatrix} V_P \\ V_B \end{bmatrix} = \begin{bmatrix} I_1 \\ I_2 \end{bmatrix} \begin{bmatrix} Z_{Sm+} Z_L & -Z_{C1} \\ -Z_{C1} & Z_{C1} + Z_{Br} \end{bmatrix}$$
 (1)

Where,  $V_P$ ,  $V_B$ ,  $Z_{Sm}$ ,  $Z_L$ ,  $Z_{C1}$  and  $Z_{Br}$  are the solar panel voltage, battery voltage, impedance of the power Sm, impedance of inductor, L, impedance of capacitor, C1 and internal impedance of battery respectively

The current flowing loop 1,  $I_1$  under first half cycle is derived from Eq. 1 and expressed in Eq.2

$$I_{1} = \frac{\begin{vmatrix} V_{P} & -Z_{C1} \\ V_{B} & Z_{C1} + Z_{Br} \end{vmatrix}}{\begin{vmatrix} Z_{Sm+}Z_{L} & -Z_{C1} \\ -Z_{C1} & Z_{C1} + Z_{Br} \end{vmatrix}} \frac{V_{P}(Z_{C1} + Z_{Br}) + V_{B}Z_{C1}}{(Z_{C1} + Z_{Br})(Z_{Sm+}Z_{L}) - Z_{C1}^{2}}$$
(2)

The current flowing at loop 2,  $I_2$  under first half cycle is also derived from Eq.1 and expressed in Eq.3

$$I_{2} = \frac{\begin{vmatrix} Z_{Sm+}Z_{L} & V_{P} \\ -Z_{C1} & V_{B} \end{vmatrix}}{\begin{vmatrix} Z_{Sm+}Z_{L} & -Z_{C1} \\ -Z_{C1} & Z_{C1+}Z_{Br} \end{vmatrix}} = \frac{V_{B}(Z_{Sm+}Z_{L}) + V_{P}Z_{C1}}{(Z_{C1} + Z_{Br})(Z_{Sm+}Z_{L}) - Z_{C1}^{2}}$$
(3)

During the second mode of DC solar charging, the power switch Sm is turned OFF, and the power diode D1becomes forward biased. The loop current I3flows along the path:

D1 $\rightarrow$ L $\rightarrow$ C1 $\rightarrow$ D1, while the loop currentI4flows through: C1 $\rightarrow$ VB $\rightarrow$ C1. The corresponding circuit configuration is shown in Fig. 4.

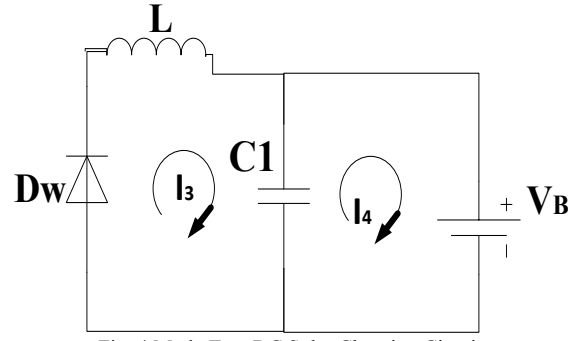


Fig. 4 Mode Two DC Solar Charging Circuit

The voltages, currents and impedances relationship of during second half cycle mode two DC solar charging condition are expressed as in Eq. (4)

$$\begin{bmatrix} -V_{c1} \\ V_B \end{bmatrix} = \begin{bmatrix} I_3 \\ I_4 \end{bmatrix} \begin{bmatrix} Z_{D1+} Z_L + Z_{C1} & -Z_{C1} \\ -Z_{C1} & Z_{C1} + Z_{Br} \end{bmatrix}$$
 (4)

The current flowing in the first loop of Fig.4 under second half cycle is expressed as

Candidus U. Eya, Chikadibia Ugwuijem Daniel and Abonyi Kingsley

$$I_{3} = \frac{\begin{vmatrix} -V_{c1} & -Z_{c1} \\ V_{B} & Z_{c1} + Z_{Br} \end{vmatrix}}{\begin{vmatrix} Z_{D1} + Z_{L} + Z_{c1} & -Z_{c1} \\ -Z_{c1} & Z_{c1} + Z_{Br} \end{vmatrix}}$$

$$= \frac{-V_{c1}(Z_{c1} + Z_{Br}) + V_{B}Z_{c1}}{(Z_{D1} + Z_{L} + Z_{c1})(Z_{c1} + Z_{Br}) - Z_{c1}^{2}}$$
(5)

The current,  $I_4$  flowing at second loop of Fig.4 under second half cycle expressed as in Eq.5

$$I_{4} = \frac{\begin{vmatrix} Z_{D1+}Z_{L} + Z_{C1} & -V_{c1} \\ -Z_{C1} & V_{B} \end{vmatrix}}{\begin{vmatrix} Z_{D1+}Z_{L} + Z_{C1} & -Z_{C1} \\ -Z_{C1} & Z_{C1} + Z_{Br} \end{vmatrix}}$$
$$= \frac{V_{B}(Z_{Sm+}Z_{L}) + V_{P}Z_{C1}}{(Z_{D1+}Z_{L}+Z_{C1})(Z_{C1}+Z_{Br}) - Z_{C1}^{2}}$$
(6)

The total charging current,  $I_{2+4}$  under solar-powered

charging condition is written in Eq. 7
$$I_{2+4} = \frac{V_B(Z_{Sm+}Z_L) + V_P Z_{C1}}{(Z_{C1} + Z_{BT})(Z_{Sm+}Z_L) - Z_{C1}^2} + \frac{V_B(Z_{Sm+}Z_L) + V_P Z_{C1}}{(Z_{D1} + Z_L + Z_{C1})(Z_{C1} + Z_{BT}) - Z_{C1}^2}$$
(7)

# C. AC Supply Charging Operation

In the AC power charging operation, a combination of uncontrolled and phase-controlled rectification is used to convert AC power into DC power. This process occurs in two phases: the single-phase positive half-cycle and the singlephase negative half-cycle. Fig.5 illustrates the AC power charging circuit, while Fig. 6 presents a simplified version for easier analysis.

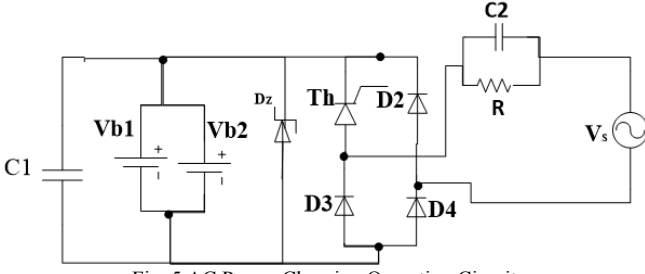


Fig. 5 AC Power Charging Operation Circuit

Fig. 6 illustrates a simplified circuit for the AC power charging operation. Vb1 and Vb2 have identical voltage ratings and are collectively represented as VB. Similarly, the impedances of C2 and Rare combined and denoted as ZCR.

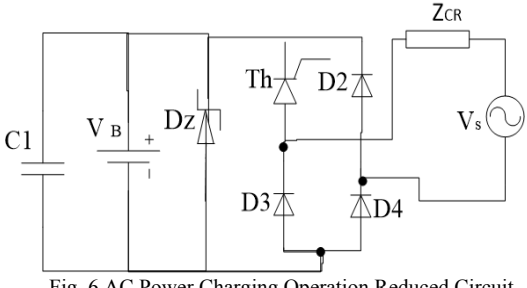


Fig. 6 AC Power Charging Operation Reduced Circuit

## 1. Single-Phase Positive Half Cycle Conduction

When the appropriate triggering signal is applied to the thyristor power switch during the positive half-cycle of the single-phase AC input, it conducts and allows current to flow. The loop currentsI5andI6follow the paths: I5:C1 $\rightarrow$ VB $\rightarrow$ C1

I6: 
$$Vs \rightarrow ZCR \rightarrow Th \rightarrow VB \rightarrow D4 \rightarrow Vs$$

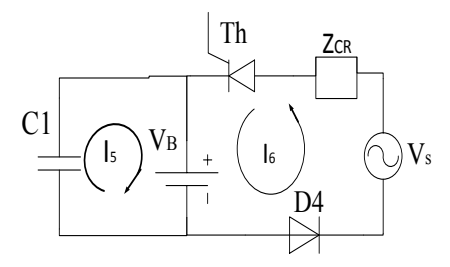


Fig. 7 Single-Phase Positive Half Cycle Circuit

During the positive half-cycle charging mode, the voltage, current, and impedance relationship is expressed in Eq. (8).

$$\begin{bmatrix} V_B \\ V_S + V_B \end{bmatrix} = \begin{bmatrix} I_5 \\ I_6 \end{bmatrix} \begin{bmatrix} Z_{C1} + Z_{Br} & -Z_{Br} \\ -Z_{Br} & Z_{Br} + Z_{Th} + Z_{CR} + Z_{D4} \end{bmatrix}$$
 (8)

Where,  $V_S$ ,  $V_B$ ,  $Z_{CR}$ ,  $Z_{Th}$  and  $Z_{D4}$  ac voltage, battery voltage, impedance of thyristor and impedance of power diode, D4 respectively.

The current, I<sub>5</sub> flowing in first loop of Fig.6 during positive half cycle is expressed as

$$I_{5} = \frac{\begin{vmatrix} V_{B} & -Z_{C1} \\ V_{S}+V_{B} & Z_{C1}+Z_{Br} \end{vmatrix}}{\begin{vmatrix} Z_{C1}+Z_{Br} & -Z_{Br} \\ -Z_{Br} & Z_{Br}+Z_{Th}+Z_{CR}+Z_{D4} \end{vmatrix}}$$
$$= \frac{V_{B}(Z_{C1}+Z_{Br})+(V_{S}+V_{B})Z_{C1}}{(Z_{C1}+Z_{Br})(Z_{Br}+Z_{Th}+Z_{CR}+Z_{D4})-Z_{Br}^{2}}$$
(9)

Also current, I<sub>6</sub> flowing in second loop of Fig.6 during positive half cycle is expressed as

$$I_{6} = \frac{\begin{vmatrix} Z_{C1} + Z_{Br} & V_{B} \\ -Z_{Br} & V_{S} + V_{B} \end{vmatrix}}{\begin{vmatrix} Z_{C1} + Z_{Br} & Z_{Br} + Z_{Th} + Z_{CR} + Z_{D4} \end{vmatrix}}$$

$$= \frac{V_{S} + V_{B}(Z_{C1} + Z_{Br}) + V_{B}Z_{C1}}{(Z_{C1} + Z_{Br})(Z_{Br} + Z_{Th} + Z_{CR} + Z_{D4}) - Z_{Br}^{2}}$$
(10)

During the single-phase negative half cycle charging mode, the power diodes, D2 and D4 are forward biased in the circuit diagram of Fig.8

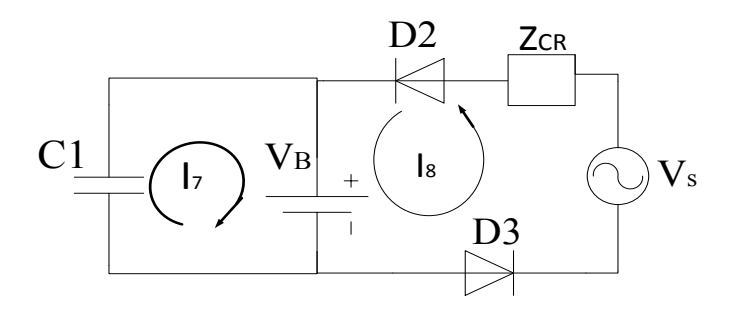


Fig. 8 Single-Phase Negative Half Cycle Circuit

Meanwhile, the voltage, current, and impedance relationship for Fig. 8 during the negative half-cycle is expressed in Eq. (11).

$$\begin{bmatrix} V_B \\ V_S + V_B \end{bmatrix} = \begin{bmatrix} I_7 \\ I_8 \end{bmatrix} \begin{bmatrix} Z_{C1} + Z_{Br} & -Z_{Br} \\ -Z_{Br} & Z_{Br} + Z_{D2} + Z_{CR} + Z_{D3} \end{bmatrix}$$
(11)

The current  $I_7$ , flowing in the first loop of Fig.7 during positive half cycle derived from Eq.11 is expressed as

$$I_7 = \frac{\begin{vmatrix} V_B & -Z_{Br} \\ |V_S + V_B & Z_{Br} + Z_{D2} + Z_{CR} + Z_{D3} \end{vmatrix}}{\begin{vmatrix} Z_{C1} + Z_{Br} & -Z_{Br} \\ -Z_{Br} & Z_{Br} + Z_{D2} + Z_{CR} + Z_{D4} \end{vmatrix}}$$

$$= \frac{V_B(Z_{Br} + Z_{D2} + Z_{CR} + Z_{D3}) + (V_S + V_B)Z_{Br}}{(Z_{C1} + Z_{Br})(Z_{Br} + Z_{D2} + Z_{CR} + Z_{D4}) - Z_{Br}^2}$$
(12)

The current  $I_8$ , flowing loop in Fig.7 during negative half cycle is expressed as

$$I_{8} = \frac{\begin{vmatrix} Z_{C1} + Z_{Br} & V_{B} \\ -Z_{Br} & V_{S} + V_{B} \end{vmatrix}}{\begin{vmatrix} Z_{C1} + Z_{Br} & -Z_{Br} \\ -Z_{Br} & Z_{Br} + Z_{Th} + Z_{CR} + Z_{D4} \end{vmatrix}}$$
$$= \frac{(V_{S} + V_{B})(Z_{C1} + Z_{Br}) + V_{B}Z_{Br}}{(Z_{C1} + Z_{Br})(Z_{Br} + Z_{D2} + Z_{CR} + Z_{D4}) - Z_{Br}^{2}}$$
(13)

The overall charging current,  $I_T$  under AC-powered charging condition is written in Eq. 14

$$I_T = I_5 + I_6 + I_8 + I_7 (14)$$

2. Design of the Rechargeable Lantern Casing for This Study

The dimensions of the rechargeable lantern casing made from a plastic bottle are stated as follows and are illustrated in Fig. 9.

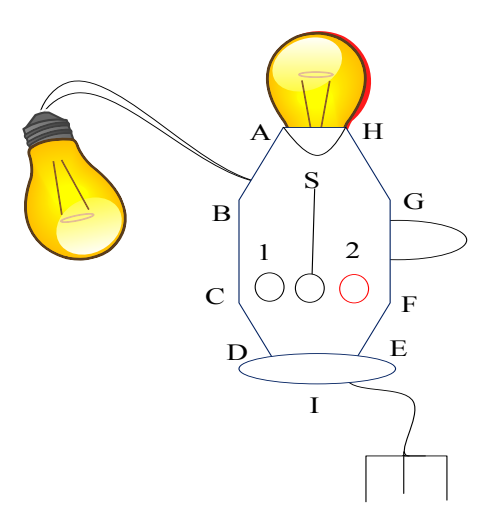


Fig. 9 Designed Dimensions of Improved Rechargeable Lantern Casing

Perimeter of the casing = 
$$AB + BC + CD + DI + IE + EF + FG + GH + HA$$
 (15)

AB = HG = 3cm; DE = 3cm, BC = GF = 4cm, CD = EF = 3cm, DI = IE = 2cm.

The perimeter of the casing is calculated using Eq. (15).

3. Input power Control strategy of the proposed system

The concept of input power control is designed such that the DC and AC power sources do not supply power simultaneously. This operation is described using the flowchart diagram shown in Fig. 10.

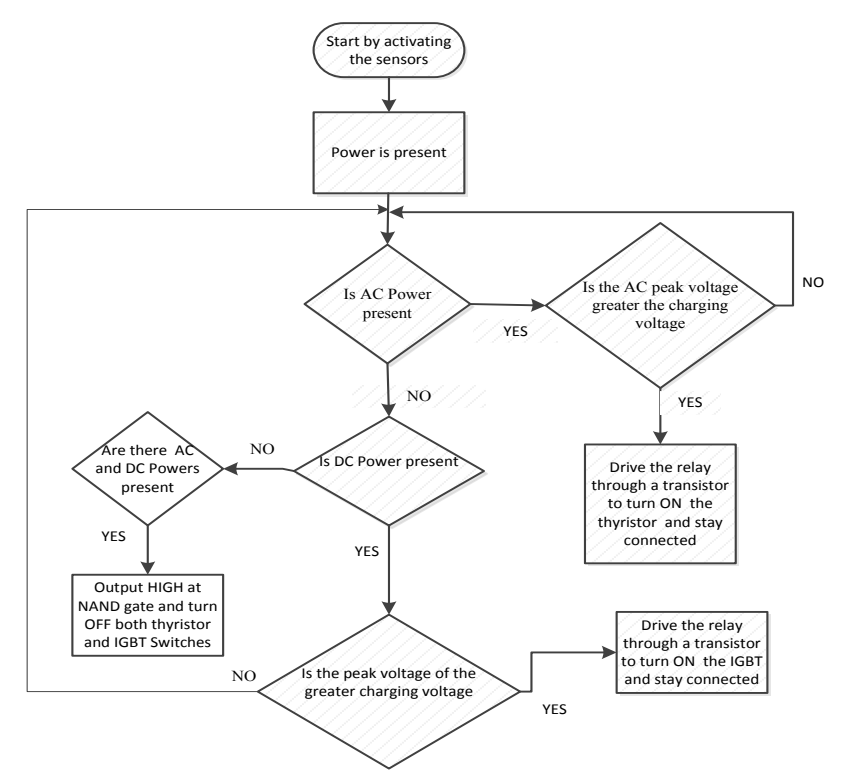


Fig. 10 Input Power Control Flow Chart

# C. Computer Simulation Model Topology

The proposed system's MATLAB/Simulink model is presented in Fig. 11.

The model comprises Simulink blocks representing nearly all the components described in Fig. 1, along with triangular and sawtooth waveform blocks.

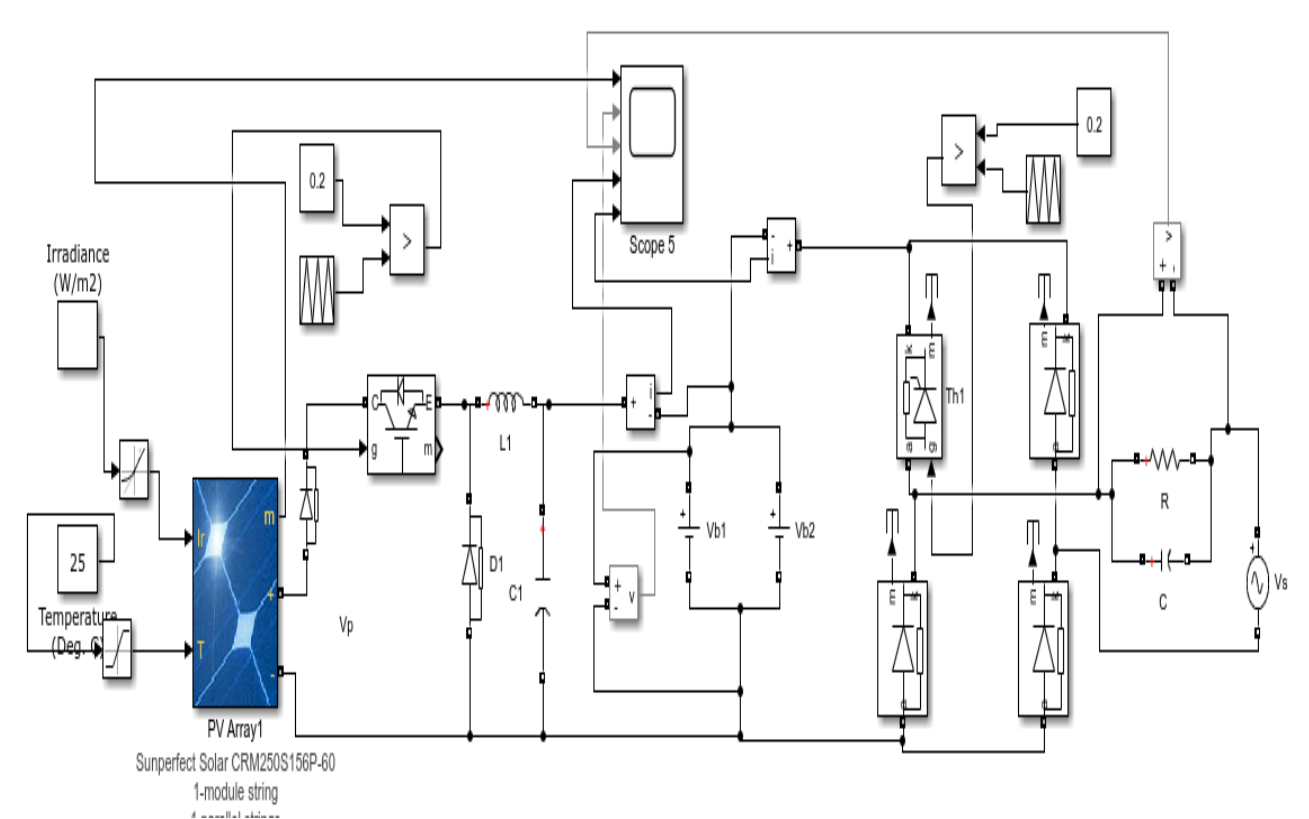


Fig. 11 MATHLAB Simulink Model of The Proposed System

#### TABLE I PARAMETERS OF THE RESEARCH SYSTEM

Components	Ratings
Inductor (Inductance)	0.2185mH
Capacitance of Capacitor	$1000.6 \times 10^{-6} F$
Solar panel ratings	30.00W
Solar panel output voltage	18.0V
Battery Capacity(lithium)	3.70V
Input AC resistance of resistor, R and non-polarized capacitor C2	47k-ohms and 475μFat 400V
Output voltage of step-down converter	4.4
Duty ratio, D	0.24
Transistors	BF 322 and BF 323
NAND gate	HD 74L500P
IGBT, thyristor, normal power diode, Zener diode and fast switching power diode	IXBH32N300, TIP120G, IN4007 and 4.7V Zener diodes, MUR 890
AC supply voltage	311-325V

## D. Simulation Results and Discussion

Figs. 12a to 12e present the simulation results of the proposed system under solar-powered charging conditions. Fig. 12a shows the solar panel voltage at 18 V. The constant charging

voltage of 4.4 V is illustrated in Fig. 12b. The power IGBT switching signal is presented in Fig. 10c, with a voltage amplitude of 1.0 V and a duty cycle of 0.24 (24%). Fig. 12d displays the battery charging current of 0.464 A, while Fig. 12e shows the voltage of the lithium-ion battery.

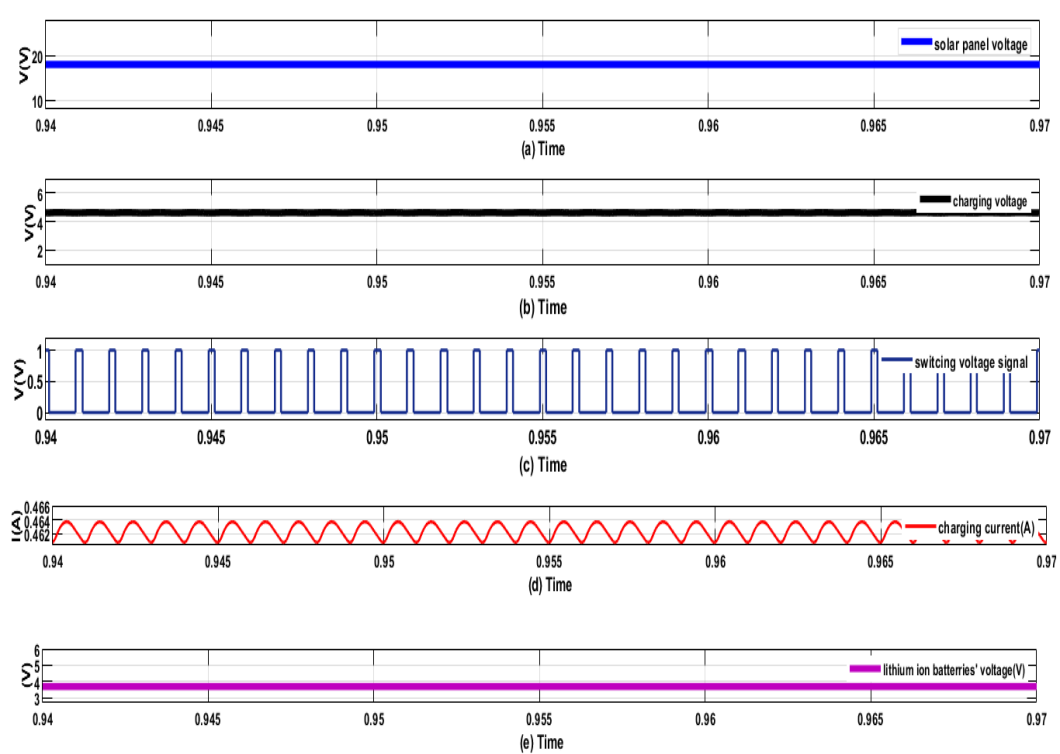


Fig. 12a Solar Panel Voltage, Fig. 12b Charging Voltage, Fig. 12c power IGBT Switching Signal, Fig. 12d Charging Current, Fig. 12e Battery Voltage

29

The simulation results of the proposed system under AC-powered charging conditions are shown in Figs. 13a to 13e.

Fig. 13a illustrates the AC supply voltage of 311 V. The reduced AC supply voltage of 6 V is presented in Fig. 13b.

Fig. 13c shows the phase-controlled rectified charging voltage of 4.4 V. Fig. 13d displays the battery charging current of 0.464 A, while Fig. 13e shows the lithium-ion battery voltage, with an amplitude of 3.7 V.

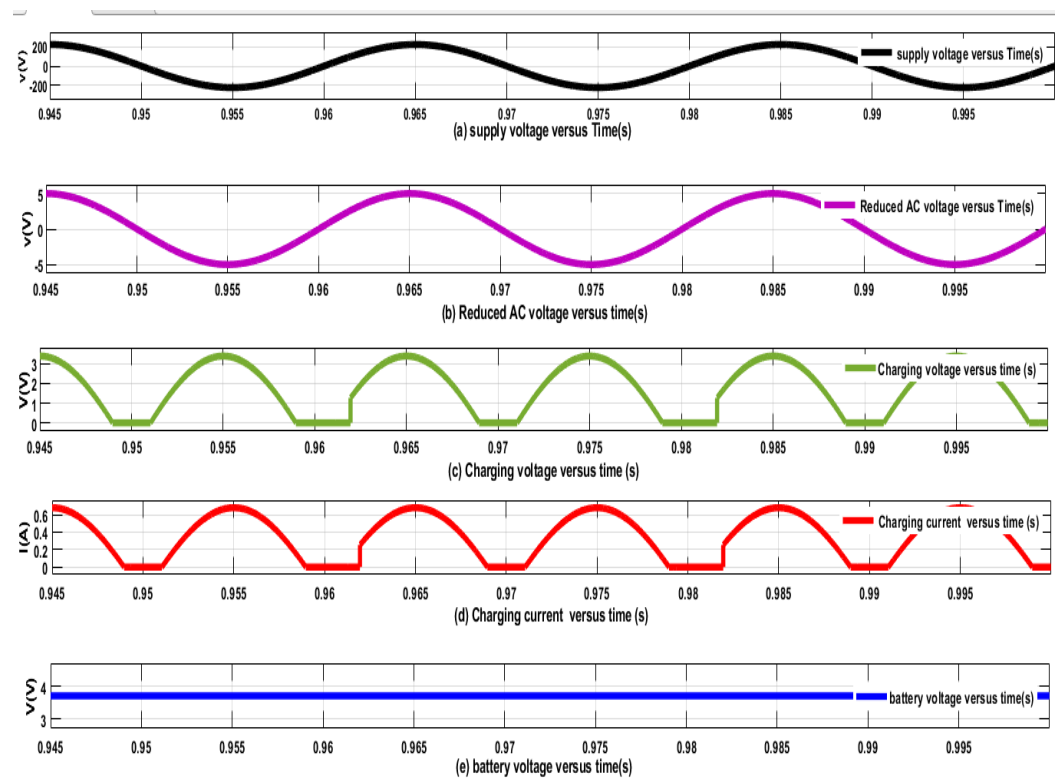


Fig. 13a AC supply voltage waveform, Fig. 13b Reduced AC supply voltage, Fig. 13c charging phase-controlled rectified voltage signal, Fig. 13d Charging Current, Fig. 13e lithium-ion battery voltage

# E. Discussion of Experimental Results of the Proposed System

Due to limited availability, two different types of digital oscilloscopes were used to obtain the experimental results.

Fig. 14 shows the solar panel voltage of 18.4 V and a switching signal with a frequency of 6.7 kHz and an amplitude of 13.4 V. The switching signal was used to trigger the gate of the IGBT.

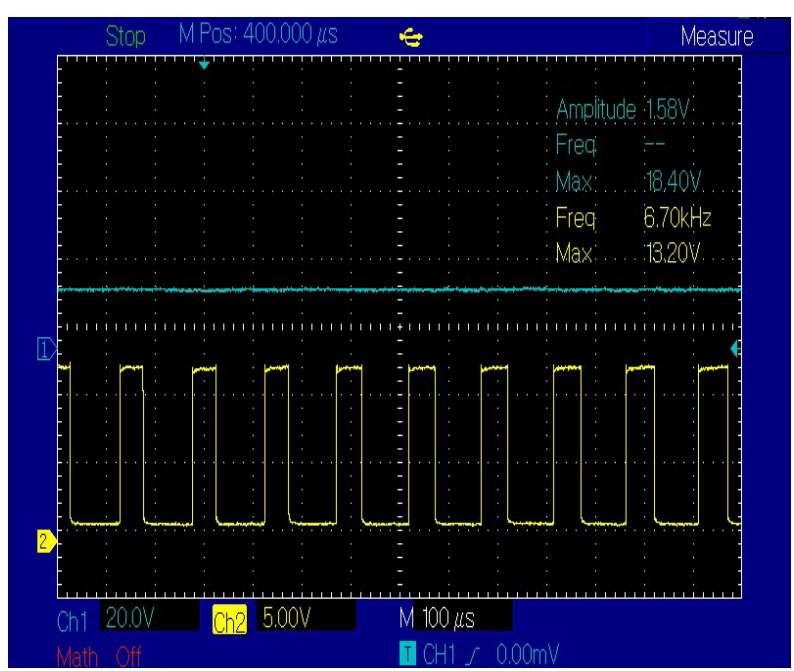


Fig. 14 Solar Panel Volage of 18.4V and Switching Signal 13.20V

Fig. 15 displays a constant charging voltage waveform with an amplitude of 4.4 V.

This waveform was used to charge two lithium-ion batteries connected in parallel.

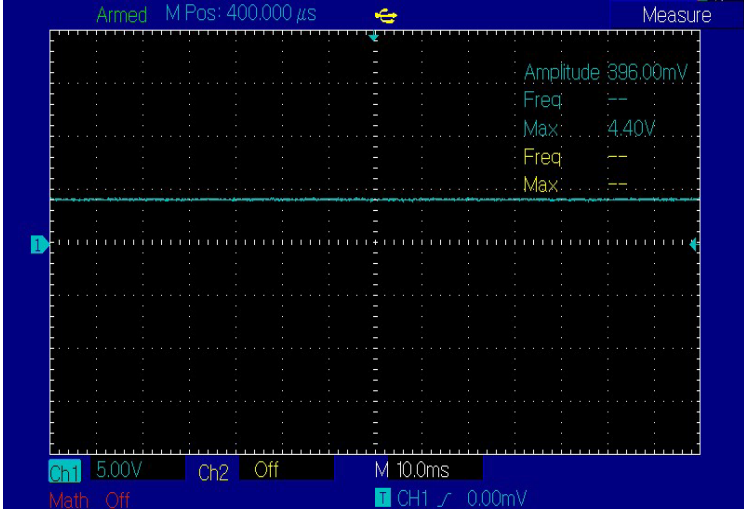


Fig. 15 Charging Voltage Waveform Under Solar Panel System

The lithium-ion battery voltage waveform under solar panel charging conditions is illustrated in Fig. 16.



Fig. 16 Lithium-ion Battery Voltage

Under AC source-based charging conditions, a supply voltage waveform of 324 V at 50 Hz is shown in Fig. 17.

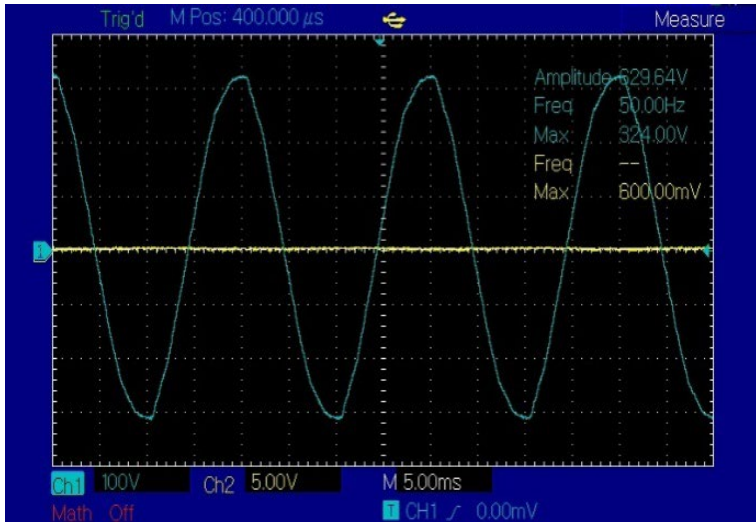


Fig. 17 AC Voltage Supply Waveform

The voltage in Fig. 17 is reduced by the action of components C and R, as previously shown in Fig. 6, and the resulting reduced AC waveform is illustrated in Fig. 18. Fig. 18

exhibits a peak value of  $6.0~\mathrm{V}$  and an operational frequency of  $49.99~\mathrm{Hz}$ .



Fig. 18 Reduced AC Voltage Supply Waveform

A phase-angle-controlled charging voltage and gate triggering waveforms are illustrated in Fig. 19. It is observed

that the charging voltage has an amplitude of 4.4 V, and the firing signals exhibit a duty ratio of 37.75%.



Fig. 19 The Charging Voltage and The Triggering Signals

Fig. 20 presents the constructed and uncoupled improved low-cost lanterns designed for upward lighting purposes.



Fig. 20 Constructed Improved and Low Cost-Low Lantern with Upward Lightening

Fig. 21 presents the constructed and uncoupled improved low-cost lanterns designed for side-lighting purposes. Fig. 22 presents an image showing measurement acquisition from the improved rechargeable lantern using a digital oscilloscope.

Fig. 23 represents the constructed and coupled improved low-cost lanterns designed for both upward and side-lighting purposes.



Fig. 21 Constructed Improved and Low Cost-Low Lantern with Upward Lightening



Fig. 22 Measuring the Voltage Level of The Batteries



Fig. 23 Completed Improved and Low Cost-Low Lantern with Upward Lightening

## VI. CONCLUSION

We have designed, modelled, and experimented with the development of an improved and low-cost rechargeable lantern for green environmental support using the

MATLAB/Simulink environment. The computer simulation results obtained from Simulink have been presented. Additionally, the experimental results, including graphs, the prototype, and real-time observations of the proposed system, have been realized.

- 1. It is evident that the system is cost-effective compared to conventional alternatives due to the following reasons:
- 2. it utilizes waste plastic materials for casing,
- 3. it reuses waste laptop batteries,
- 4. it supports dual charging via both solar panels and AC supply through appropriate switching, and it helps reduce environmental pollution by minimizing plastic waste.

## VII. FUTURE WORK

We aim to adopt 3D printing technology for packaging purposes and incorporate wireless monitoring and control capabilities.

#### **ACKNOWLEDGEMENT**

The authors sincerely acknowledge the Federal Ministry of Communication, Innovation, and Digital Economy (FMCIDE) and the National Information Technology Development Agency (NITDA) for their vital support in advancing this research. This support is instrumental in progressing our research endeavours and contributing to the development of the AI landscape in Nigeria

#### **Declaration of Conflicting Interests**

The authors declare no potential conflicts of interest with respect to the research, authorship, and/or publication of this article.

#### Funding

This work was funded by NITDA, in collaboration with FMCIDE, under the Nigerian Artificial Intelligence Research Scheme (NAIRS), Grant No. NITDA/HQ/RG/AI2939622426.

# Use of Artificial Intelligence (AI)-Assisted Technology for Manuscript Preparation

The authors confirm that no AI-assisted technologies were used in the preparation or writing of the manuscript, and no images were altered using

#### REFERENCES

- [1] M. P. Blimpo and Malcolm, "Design and development of costeffective solar rechargeable LED lantern," *Int. J. Innov. Sci. Res. Technol.*, vol. 6, no. 3, pp. 1168-1170, Mar. 2021. [Online]. Available:https://www.researchgate.net/publication/352865498\_Design\_and\_Development\_of\_Cost-Effective\_Solar\_Rechargeable\_Led\_Lantern. doi: 10.1596/978-1-4648-1361-0. [Accessed: Mar. 30, 2025].
- [2] D. T. Barki and G. B. Habbu, "Creating global awareness for eliminating light poverty in the world: To replace hazardous kerosene lamps with clean and safe solar lamps," in *Proc. 33rd IEEE Photovolt. Spec. Conf. (PVSC)*, 2008, pp. 1-5. doi: 10.1109/PVSC.2008.4922825.
- [3] C. Nagarajan, B. Tharani, S. Saravanan, and M. Muruganandam, "Performance analysis of hybrid multi-port AC-DC/DC-DC embedded based energy flow optimizing using resilient power flow control (RPFC) technique," *Asian J. Electr. Sci.*, vol. 10, no. 2, pp. 16-28, 2021. doi: 10.51983/ajes-2021.10.2.3039. [Accessed: May 30, 2025].
- [4] N. A. Priya, M. Aswin, S. J. A. Shane, Y. B. Dino, and D. Dagul, "Performance analysis of a high gain LUO converter-based hybrid PV-wind system," *Asian J. Electr. Sci.*, vol. 10, no. 1, pp. 1-4, 2021. doi: 10.51983/ajes-2021.10.1.2794.
- [5] P. K. Sahu, "Performance analysis of different tie-line for synchronization of 12-area two interconnected thermal power grid," *Asian J. Electr. Sci.*, vol. 6, no. 2, pp. 37-50, 2017. doi: 10.51983/ajes-2017.6.2.1997.
- [6] A. Abebe, A. Pushparaghavan, and E. Gedefaye, "A study on optimal design feasibility of microgrid power system for rural electrification: Amhara Region in Ethiopia," *Asian J. Electr. Sci.*, vol. 8, no. 3, pp. 26-30, 2019. doi: 10.51983/ajes-2019.8.3.2064.
- [7] P. L. Mangeshkar and T. G. Manohar, "Design and analysis of optimal maximum power point tracking algorithm using ANFIS controller for PV systems," *Asian J. Electr. Sci.*, vol. 8, no. 3, pp. 11-17, 2019. doi: 10.51983/ajes-2019.8.3.2103.
- [8] B. S. V. Prabhu and M. Suresh, "Applications of solar lantern systems-A review," in *Proc. IEEE Int. Conf. Comput. Intell. Comput. Res.* (ICCIC), 2016. doi: 10.1109/ICCIC.2016.7919702. [Accessed: Mar. 29, 2025].
- [9] B. M. Prabhakar, J. Ramprabhakar, and V. Sailaja, "Estimation and controlling the state of charge in battery augmented photovoltaic system," in *Proc. Power Energy Syst.: Towards Sustain. Energy* (PESTSE), Bangalore, India, 2016. [Online]. Available: https://ieeexplore.ieee.org/document/7516431. doi: 10.1109/PESTSE. 2016.7516431.
- [10] K. Bathirappan, K. Kumar, and D. Subaranjani, "Solar powered battery charging with reverse current protection system," *Int. J. Sci. Res. Eng. Manag.*, vol. 8, no. 9, pp. 1-8, 2024. doi: 10.55041/IJSREM37657.
- [11] T. L. Gibson and N. A. Kelly, "Solar photovoltaic charging of lithiumion batteries," *J. Power Sources*, vol. 195, no. 12, pp. 3928-3932, Jun. 2010. doi: 10.1016/j.jpowsour.2009.12.082.